

Dewetting of Ultrathin Solid Films

O. Pierre-Louis,^{1,2,3} A. Chame,⁴ and Y. Saito⁵

¹*LPMCN, Université Lyon 1, 43 Boulevard du 11 novembre, 69622 Villeurbanne, France*

²*Laboratoire de Spectrométrie Physique, UJF Grenoble 1, BP 87, 38402 St Martin d'Hères, France*

³*Rudolf Peierls Centre for Theoretical Physics, 1 Keble Road, Oxford OX1 3NP, United Kingdom*

⁴*Universidade Federal Fluminense, Avenida Litorânea s/n, 24210-340 Niterói RJ, Brazil*

⁵*Keio University, 3-14-1, Hiyoshi, Kohoku-ku, Yokohama, Kanagawa, 223-8522 Japan*

(Received 25 August 2009; published 4 November 2009)

Ultrathin crystalline solid films are found to dewet with a faceted rim. In the case of heterogeneous dewetting initiated from a linear trench or from periodically arranged holes, the dewetted area expands either with a faceted multilayer rim or in a layer-by-layer fashion. In the case of homogeneous dewetting, holes are accompanied with multilayer rims and the uncoverage increases as a power law of time. Results of kinetic Monte Carlo simulations are elucidated within the frame of nucleation theory and surface diffusion limited dynamics.

DOI: 10.1103/PhysRevLett.103.195501

PACS numbers: 81.10.Aj, 05.70.Ln, 68.55.-a

Solid films with submicron thicknesses may break up into islands to lower their energy. Such a “dewetting” process was observed in many experimental systems [1–6]. Up to now, the theoretical analysis of solid-film dewetting has been based on the Mullins continuum model for surface diffusion [7]. This approach predicts the formation of a smooth dewetting rim at the edge of the film, with scaling laws for the increase of the radius of a hole $\sim t^{1/4}$ [8], and for the position of straight fronts $\sim t^{2/5}$ [9]. However, the presence of facets, the evolution of which is controlled by 2D nucleation, leads to novel phenomena which cannot be accounted for within the frame of the Mullins model. Examples include the relaxation of nanocrystals [10,11], the drift of islands on vicinal substrates [12], layer-by-layer dewetting of ice islands [13], or the formation of labyrinthine patterns of bilayer islands during the dewetting of a monolayer [14].

In this Letter, we show that the dewetting of solid films from two to several atomic layers thick is drastically affected by the presence of facets. The results of our kinetic Monte Carlo (KMC) simulations agree with an analysis based on 2D nucleation theory and diffusion-limited dynamics. When dewetting is heterogeneous, i.e., dewetting is initiated at preexisting holes, or at the film edge, two regimes are obtained. A regime with a faceted multilayer rim, where the front position scales as $t^{1/2}$, and a layer-by-layer dewetting regime where a monolayer island nucleated far from the dewetting front invades the whole film. In contrast, during homogeneous dewetting, where holes arise from fluctuations in a perfect and clean system, multilayer rims always form.

We use the solid on solid KMC model of Ref. [14]. On a square lattice with lattice unit a and periodic boundary conditions, the local height is $z \geq 0$. The substrate surface, at $z = 0$, is flat and frozen. Epilayer atoms hop to nearest neighbor sites with rates $\nu_0 e^{-E/T}$, where ν_0 is an attempt frequency, and T is the temperature (in units with $k_B = 1$).

The hopping barrier is $E = nJ - \delta_{z,1}E_S$, where n is the number of in-plane nearest neighbors, J is the bond energy, δ is the Kronecker symbol, and E_S is the adsorbate-substrate excess energy. Our energy unit is J , so that $J = 1$. When $E_S \gg 1$, the energy is minimized by creating high islands [14]. When $E_S \rightarrow 0$ the epilayer spreads on the substrate. We choose $0.3 < T < 0.6$, high enough to allow for significant mass transport, but lower than the roughening temperature so that facets are present (as in typical dewetting experiments).

Heterogeneous dewetting.—In our first type of initial condition, a straight trench is drawn throughout a film of thickness h along the (01) axis, hereafter denoted as y . One of the two straight dewetting fronts is shown in Fig. 1(a). The fronts move in opposite directions so as to increase the width of the trench. For large E_S and small h , a multilayer rim forms. As shown on Fig. 1(a), each additional layer in the rim is formed after the previous one has been completed, so that the rim is faceted. The density of nucleation events decreases rapidly with the height of the rim, and in the late stages, only one nucleation event occurs for the formation of a new layer.

We shall now propose a model for the evolution of the rim height h_1 , the position of the film edge x_1 , and of the rim width $\ell = x_2 - x_1$. Assuming diffusion-limited mass transport on the rim facet, and translational invariance along y , we expect

$$h_1 \partial_t x_1 = -a^2 D \partial_x c(x_1) + (x_2 - x_1) \partial_t h_1, \quad (1)$$

$$(h_1 - h) \partial_t x_2 = -a^2 D \partial_x c(x_2), \quad (2)$$

where D and $c(x)$ are the diffusion constant and concentration of adatoms on the rim facet. The last term in Eq. (1) accounts for the possible nucleation of new layers. On the rim facet, where $x_1 \leq x \leq x_2$, c obeys a quasistatic diffusion equation $D\Delta c = 0$. We assume local equilibrium with concentrations $c_{\text{eq}}(1 + \sigma)$ at x_1 , and c_{eq} at x_2 . Model

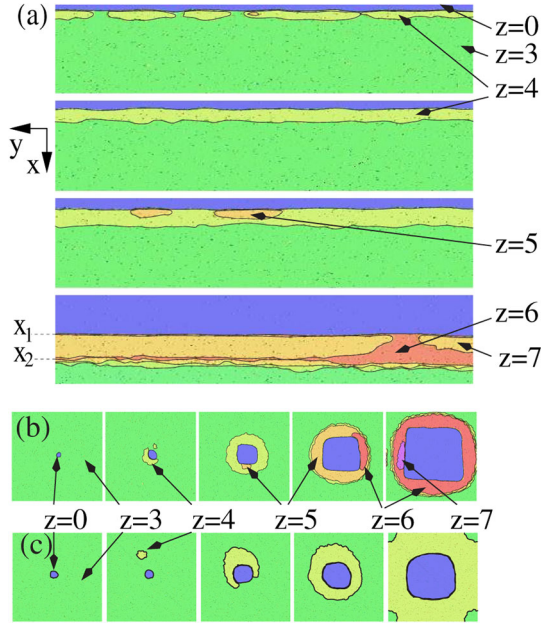


FIG. 1 (color online). KMC simulations with $T = 0.4$ and $h = 3$. Black lines indicate atomic steps. (a) Detail of the initial stages of a 600×1000 simulation with $E_s = 0.5$. A faceted rim forms. (b),(c) Dewetting from one hole in a 400×400 system. (b) A rim forms at $E_s = 0.4$. (c) Layer-by-layer dewetting at $E_s = 0.25$.

parameters are related to the KMC parameters: $D = a^2 \nu_0 / 4$, and $c_{\text{eq}} = a^{-2} e^{-2/T}$ [14]. Moreover, local equilibrium at x_1 imposes $\sigma = \exp[E_s / h_1 T] - 1$.

Combining Eqs. (1) and (2), we obtain mass conservation as

$$x_1 h = (x_2 - x_1)(h_1 - h) + C, \quad (3)$$

where C is a constant. On the rim facet, $\partial_x c(x) = -c_{\text{eq}} \sigma / \ell$, so that using Eqs. (1) and (2), x_1 can be written as a function of h_1 :

$$x_1 = \frac{C}{h} + (2a^2 D c_{\text{eq}})^{1/2} H_1^{-1} \left(\int_{t_0}^t dt' H_1' \sigma' \right)^{1/2}, \quad (4)$$

where $H_1 = (h^{-1} - h_1^{-1})^{-1}$, t_0 is a constant, and $'$ indicates that $t \rightarrow t'$.

The rim height h_1 increases via the nucleation of new layers on the rim facet. The typical distance between nucleation events is $L_{\text{nuc|zip}} = (V_{\text{zip}} / \mathcal{J})^{1/2}$, where \mathcal{J} is the monolayer island nucleation rate per unit rim length, and V_{zip} is the zipping velocity of the monolayer along the rim. When the system length L along y is larger than $L_{\text{nuc|zip}}$, multiple nucleation events occur on the top facet, and we expect $\partial_t h_1 = (V_{\text{zip}} \mathcal{J})^{1/2}$. In the single nucleation regime where $L < L_{\text{nuc|zip}}$, we expect $\partial_t h_1 = L \mathcal{J}$. As a summary:

$$\partial_t h_1 = \mathcal{J} \min[L, L_{\text{nuc|zip}}] = \min[L \mathcal{J}, (V_{\text{zip}} \mathcal{J})^{1/2}]. \quad (5)$$

The next paragraphs are devoted to the evaluation of \mathcal{J} and V_{zip} . Let us start with \mathcal{J} . The local chemical potential

on the rim facet is $\Delta\mu \approx T(c/c_{\text{eq}} - 1)$. Since the KMC temperature is high, the step tension γ is isotropic and a small nucleating island is circular with a radius r . Assuming $r \ll x_2 - x_1$, the island Gibbs free energy reads: $G = 2\pi r \gamma - \pi r^2 \Delta\mu / a^2$. The island critical radius is $r_c = \gamma a^2 / \Delta\mu$, and the nucleation barrier is $G_c = \pi \gamma^2 a^2 / \Delta\mu$. The nucleation rate per unit area is then given by the standard relation [15]

$$I = a^{-2} \Gamma_{+c} \left(\frac{-G_c^{(2)}}{2\pi T} \right)^{1/2} e^{-G_c/T}, \quad (6)$$

where $\Gamma_{+c} = 2\pi r_c c(x) D / a$ [14] is the rate of attachment of atoms to the island when $r = r_c$, and $G_c^{(2)}$ is the second derivative of G with respect to the number of atoms in the island, at $r = r_c$. In the limit $E_s \ll Th_1$, and $TE_s \ll \pi \gamma^2 a^2 h_1$, the rate $\mathcal{J} = \int_{x_1}^{x_2} dx I$ reads

$$\mathcal{J} = \ell \frac{D c_{\text{eq}}}{a^2} \left(\frac{E_s}{Th_1} \right)^{3/2} \left(\frac{T^2}{\pi \gamma^2 a^2} \right) e^{-\pi \gamma^2 a^2 h_1 / (TE_s)}, \quad (7)$$

where $\ell = x_2 - x_1$ is a function of h_1 from Eqs. (3) and (4).

We turn to the evaluation of V_{zip} . The only available length scale for a monolayer island on the rim facet growing along the dewetting front as in Fig. 1(a) is the monolayer edge curvature κ . We therefore expect:

$$V_{\text{zip}} \sim a^2 D c_{\text{eq}} \kappa \left(\frac{E_s}{Th_1} - \frac{a^2 \gamma \kappa}{T} \right). \quad (8)$$

The selected curvature is the one which maximizes the velocity: $\kappa = E_s / (2a^2 \gamma h_1)$, so that

$$V_{\text{zip}} \approx C_{\text{zip}} a^2 D c_{\text{eq}} \frac{E_s^2}{a^2 Th_1^2 \gamma}, \quad (9)$$

where C_{zip} is an unknown number. Measurements from KMC simulations in a 1000×1000 system with $h_1 = 7$ and 8 indicate that $C_{\text{zip}} \approx 0.25 \pm 0.05$ [16].

Using Eqs. (7) and (9) to evaluate $L_{\text{nuc|zip}}$, the transition from multiple to single nucleation event per layer at $L = L_{\text{nuc|zip}}$ is obtained for $h_1 \approx 6.5$ when $L = 1000$, $E_s = 0.5$, and $T = 0.4$, in good agreement with KMC. The evolutions of h_1 and x_1 are obtained by numerically solving Eqs. (4) and (5) with $C = 0$ and $t_0 = 0$ (corresponding to $x_1 = x_2 = 0$ at $t = 0$). The solution is seen to agree quantitatively with KMC in Fig. 2(a) (simulations with $h = 4$ give similar results). This agreement relies on the accurate effective value $\gamma \approx 0.42$ at $T = 0.4$, extracted from the Ising model [14,17]. Finally, since the increase of h_1 slows down exponentially from Eqs. (5) and (7), one obtains $x_1 \sim t^{1/2}$ from Eq. (4) in the late stages.

Our second type of initial condition for KMC simulations mimics heterogeneous dewetting from holes resulting either from lithography or heterogeneous nucleation. We start with a periodic array of holes in a film of thickness $z = h$, using a square periodic box of size L_H with one hole. The initial hole diameter is much smaller than L_H , but larger than the hole critical size, so that the hole grows irreversibly. A faceted multilayer rim forms for large E_s ,

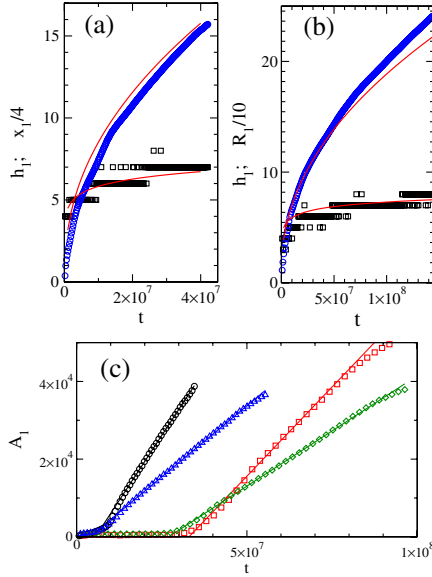


FIG. 2 (color online). (a) Position x_1 and rim height h_1 for a straight front. Symbols: KMC with $L = 1000$, $T = 0.4$, $E_S = 0.5$, $h = 3$. Solid lines: model Eqs. (4) and (5). h_1 saturates, whereas $x_1 \sim t^{1/2}$ asymptotically. (b) A similar behavior is found for the rim height h_1 and radius R_1 of a hole. Symbols: KMC with $L_H = 800$, $A_0 = 225$, $T = 0.4$, $E_S = 0.5$, and $h = 3$. Solid lines: numerical solution of Eqs. (10), (11), and (14). (c) Area A_1 of a hole in the presence of a monolayer rim. KMC with $L_H = 400$, $T = 0.4$, and various (E_S, h, A_0) : \circ (0.2, 2, 144); \square (0.17, 2, 144); \diamond (0.25, 3, 576); \triangle (0.3, 3, 576). Solid line: Eq. (16) with $A_1 = \pi R_1^2 \sim t$ and a prefactor between 0.88 and 1.15.

small h , and large L_H . The resulting evolution is reported in Fig. 1(b). Following the same lines as for the straight front, we obtain a model for the dynamics of a circular rim around a hole. The variables are now R_1 , the hole radius, and R_2 , the hole plus rim radius. Solving the diffusion equation on the rim leads to

$$h_1 \partial_t R_1^2 = \frac{4a^2 D c_{\text{eq}} \sigma}{\ln(R_2/R_1)} + (R_2^2 - R_1^2) \partial_t h_1, \quad (10)$$

and mass conservation reads

$$h \pi R_1^2 = (h_1 - h)(\pi R_2^2 - \pi R_1^2) + C_A. \quad (11)$$

In the late stages when $R_1 \gg (C_A/\pi h)^{1/2}$, one finds

$$R_1^2 \approx 4a^2 D c_{\text{eq}} \frac{h_1 - h}{h_1} \int_0^t \frac{dt' \sigma'}{(h_1' - h) \ln[h_1'/(h_1' - h)]}. \quad (12)$$

The total nucleation rate on the top facet is $\mathcal{K} = \int_{R_1}^{R_2} dr 2\pi r I(r)$. From Eq. (6) in the limit $E_S \ll Th_1$, and $2TE_S \ln[R_2/R_1] \ll \pi\gamma^2 a^2 h_1$, we obtain

$$\mathcal{K} = \frac{2R_2^2}{a^4} \ln\left[\frac{R_2}{R_1}\right] D c_{\text{eq}} \frac{T^{1/2} E_S^{3/2}}{h_1^{3/2} \gamma^2} e^{-\pi\gamma^2 a^2 h_1/(TE_S)}. \quad (13)$$

From an analogy to Eq. (5) when $R_2 - R_1 \ll R_1$, we have

$$\partial_t h_1 = \min\left[\mathcal{K}, \left(\frac{V_{\text{zip}} \mathcal{K}}{2\pi R_1}\right)^{1/2}\right]. \quad (14)$$

The numerical solution of Eqs. (10), (11), and (14) with $R_1 = R_2 = (A_0/\pi)^{1/2}$ at $t = 0$, shown in Fig. 2(b), is in good agreement with the simulations. Since the evolution of h_1 slows down exponentially with time from Eqs. (13) and (14), one finds $R_1 \sim R_2 \sim t^{1/2}$ for large times from Eq. (12).

For smaller E_S , larger h , and smaller L_H , a different regime is observed in KMC simulations. The case of a hole in a square box is shown on Fig. 1(c). Two-dimensional nucleation usually occurs far from the dewetting front. After nucleation, the monolayer island grows, closes around the hole, and invades the whole film. The process is repeated, and the increase of the film height thus proceeds in a layer-by-layer fashion. A similar regime exists for straight fronts, but we shall restrict the discussion to the case of holes.

Comparing the island nucleation time $1/(IL_H^2)$ and the concentration relaxation time L_H^2/D , nucleation is found to occur anywhere on the film with equal probability if $L_H < L_{\text{far}}$, and in the vicinity of the hole if $L_H > L_{\text{far}}$, with $L_{\text{far}} = (D/I)^{1/4}$. Assuming that the chemical potential is homogeneous on the film, we have $\Delta\mu = E_S/(Th)$, so that using Eq. (6):

$$L_{\text{far}} = \frac{c_{\text{eq}}^{1/4}}{a^{1/2}} \left(\frac{E_S}{Th}\right)^{1/8} e^{\pi\gamma^2 a^2 h/(4E_S T)}. \quad (15)$$

The nucleated monolayer island then grows by mass transfer from the hole, reaches the hole, and closes around it (with velocity V_{zip}). After the rim closure, the evolution is modeled by a circular monolayer rim. From Eq. (12) with $h_1 = h + 1$ and $\partial_t h_1 = 0$, we obtain

$$R_1 \approx 2a \left(\frac{D c_{\text{eq}} \sigma}{(h+1) \ln[h+1]} t \right)^{1/2}. \quad (16)$$

In Fig. 2(c), Eq. (16) is seen to agree with KMC simulations up to a prefactor of about 15%, even though the monolayer rim is not perfectly circular.

Before the monolayer rim has invaded the whole film, a new island will be nucleated above it if $\int_0^{t_{\text{inv}}} dt \mathcal{K} > 1$, where t_{inv} is the time for the monolayer rim to invade the whole system. This condition is rewritten as $\int_{R_0}^{L_H} dR_1 \mathcal{K}(R_1)/\partial_t R_1 > 1$, where R_0 is the initial hole radius. Using Eqs. (13) and (16) in the limit $R_0 \ll L_H$, we find that nucleation occurs on the monolayer rim before it has invaded the full system if $L_H > L_2$, with

$$L_2 = \frac{2^{3/4} \pi^{1/2} a^{3/2} \gamma^{1/2} e^{\pi\gamma^2 a^2 (h+1)/(4E_S T)}}{E_S^{1/8} T^{3/8} (h+1)^{1/8} \ln[h+1]^{1/2}}. \quad (17)$$

Choosing $T = 0.4$, $h = 3$, and $L_H = 400$, Eqs. (15) and (17) indicate a narrow transition. Indeed, $L_{\text{far}}, L_2 > L_H$ when $E_S < 0.21$, and $L_{\text{far}}, L_2 < L_H$ when $E_S > 0.27$. This is in qualitative agreement with KMC simulations, where a layer-by-layer regime with a single nucleation event far from the hole is found for $E_S \leq 0.25$, and a multilayer rim forms for $E_S \geq 0.35$.

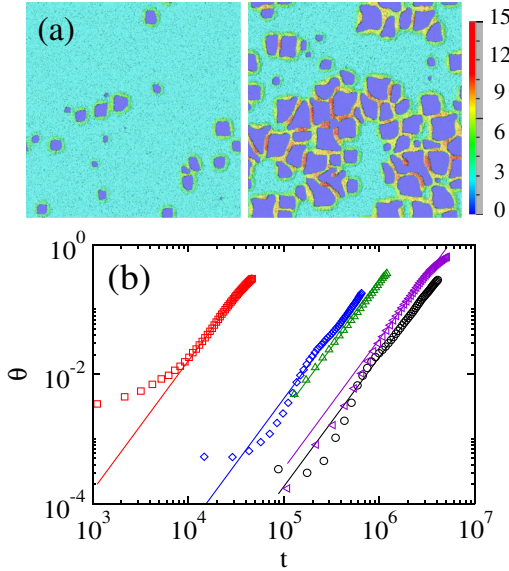


FIG. 3 (color online). (a) Snapshots of a 1000×1000 KMC simulation, with $h = 3$, $T = 0.5$, and $E_s = 0.7$, at $t = 1.6 \times 10^6$, and 4.1×10^6 . (b) Uncoverage in KMC during homogeneous dewetting. Solid lines are guides to the eye $\sim t^2$. Symbols represent KMC simulation with $h = 2$ and (T, E_s) : \circ (0.4, 0.5); \square (0.5, 0.7); \diamond (0.4, 0.7); \triangle (0.5, 0.3); System sizes are 600×600 or 400×400 . \triangleleft correspond to the parameters of (a).

Homogeneous Dewetting.—Starting from a perfect layer of height h , we wait for the spontaneous formation of holes, and monitor the subsequent dewetting process shown in Fig. 3(a). The hole nucleation rate is $I_H \sim e^{-G_{Hc}/T}$, where G_{Hc} is the hole nucleation barrier. Assuming that the hole edge is a bunch of h noninteracting atomic steps, one finds $G_{Hc} \approx \pi h^2 a^2 \gamma^2 / E_s$. The area of a hole is growing as $A = f(t_A)$, where t_A is the time since the birth of the hole. From Eq. (12), $f(t) \approx D_H t$, where D_H is a constant. Thus, the typical distance between holes $L_{H-H} \sim (D_H / I_H)^{1/4} \sim e^{\pi h^2 a^2 \gamma^2 / 4 E_s T}$ is much larger than $L_2 \sim e^{\pi(h+1)a^2 \gamma^2 / 4 E_s T}$ when $h > 1$. Hence, multilayer rims always form in homogeneous dewetting when $h > 1$.

Let us define the uncoverage θ as the fraction of the substrate uncovered by the dewetting process. In the early stages, before the holes come into contact $\theta \approx I_H \int_0^t dt' f(t')$. Since $f(t) \approx D_H t$, we expect $\theta \sim t^2$. In Fig. 3(b), this scaling law is seen to be in good agreement with the simulations.

In the presence of preexisting holes with a periodicity L_H , dewetting is expected to be predominantly heterogeneous when $L_H \ll L_{H-H}$, and homogeneous when $L_H \gg L_{H-H}$. Though L_{H-H} depends on the hole nucleation barrier G_{Hc} whose quantitative expression is missing, the approximation mentioned above $G_{Hc} \approx \pi h^2 a^2 \gamma^2 / E_s$ correctly predicts that homogeneous nucleation dominates for small h and large E_s , in qualitative agreement with KMC simulations.

Four remarks are in order. First, the dewetting dynamics with $h \geq 2$ not only differs from the results of the Mullins

model, it also differs from the dewetting of a monolayer ($h = 1$), where the motion of a straight front and the opening of dewetting zones proceed at constant velocity, i.e., they both scale as t , so that $\theta \sim t^3$ [14].

Second, the analysis of the Mullins model in the literature has revealed two instabilities: (i) the formation of holes behind the rim [1,9]; (ii) the breakup of the rim via a Rayleigh-Plateau-like pinching [18]. The latter is a candidate for the initiation of fingers observed in SOI (Si/SiO₂) systems [2]. But no instability was observed in our simulations, in agreement with experiments with SOI systems [4], where no trace of the instability was found for $h < 4$ nm. These results show that the instabilities do not have enough time to develop before holes meet in very thin films.

Third, we have assumed diffusion-limited dynamics, but attachment-detachment at atomic steps could be the limiting process at lower temperatures, as in Ref. [14]. Different scaling laws are then expected.

Finally, we have discussed dewetting starting from holes. By analogy, we expect similar regimes for islands of lateral size L_H . For a given height, small islands should dewet in a layer-by-layer fashion, while large ones should exhibit multilayer dewetting rims. The former regime was observed recently in the dewetting of ice films [13].

As a conclusion, we have investigated the dewetting of ultrathin solid films. The faceting of the rims leads to a characteristic $t^{1/2}$ power-law for the motion of dewetting fronts. A layer-by-layer dewetting regime was found to occur only for heterogeneous dewetting with small distances between the preexisting holes.

We acknowledge support from “nanomorphogénèse” and “DéFiS” ANR-PNANO grants, and from JSPS grants.

-
- [1] E. Jiran and C. Thompson, *Thin Solid Films* **208**, 23 (1992).
 - [2] B. Yang *et al.*, *Phys. Rev. B* **72**, 235413 (2005).
 - [3] B. Krause *et al.*, *J. Chem. Phys.* **119**, 3429 (2003).
 - [4] Z. Burhanudin *et al.*, *Thin Solid Films* **508**, 235 (2006).
 - [5] R. Saxena *et al.*, *Phys. Rev. B* **72**, 115425 (2005).
 - [6] M. Coll *et al.*, *Phys. Rev. B* **73**, 075420 (2006).
 - [7] W. Mullins, *J. Appl. Phys.* **28**, 333 (1957).
 - [8] D. Srolovitz and S. Safran, *J. Appl. Phys.* **60**, 255 (1986).
 - [9] H. Wong *et al.*, *Acta Mater.* **48**, 1719 (2000).
 - [10] N. Combe, P. Jensen, and A. Pimpinelli, *Phys. Rev. Lett.* **85**, 110 (2000).
 - [11] W. Mullins and G. S. Rohrer, *J. Am. Ceram. Soc.* **83**, 214 (2000).
 - [12] W. Ling *et al.*, *Surf. Sci. Lett.* **570**, L297 (2004).
 - [13] K. Thürmer and N.C. Bartelt, *Phys. Rev. Lett.* **100**, 186101 (2008).
 - [14] O. Pierre-Louis, A. Chame, and Y. Saito, *Phys. Rev. Lett.* **99**, 136101 (2007).
 - [15] See, e.g., Y. Saito, *Statistical Physics of Crystal Growth* (World Scientific, Singapore, 1996).
 - [16] The measurement is actually indirect, and will be discussed in detail elsewhere.
 - [17] B. Krishnamachari *et al.*, *Phys. Rev. B* **54**, 8899 (1996).
 - [18] W. Kan and H. Wong, *J. Appl. Phys.* **97**, 043515 (2005).